Article

# Conformations of Laulimalide in DMSO-*d*

Pahk Thepchatri, Daniel O. Cicero, Edith Monteagudo, Arun K. Ghosh, Ben Cornett, Eric R. Weeks, and James P. Snyder

*J. Am. Chem. Soc.*, **2005**, 127 (37), 12838-12846• DOI: 10.1021/ja042890e • Publication Date (Web): 25 August 2005



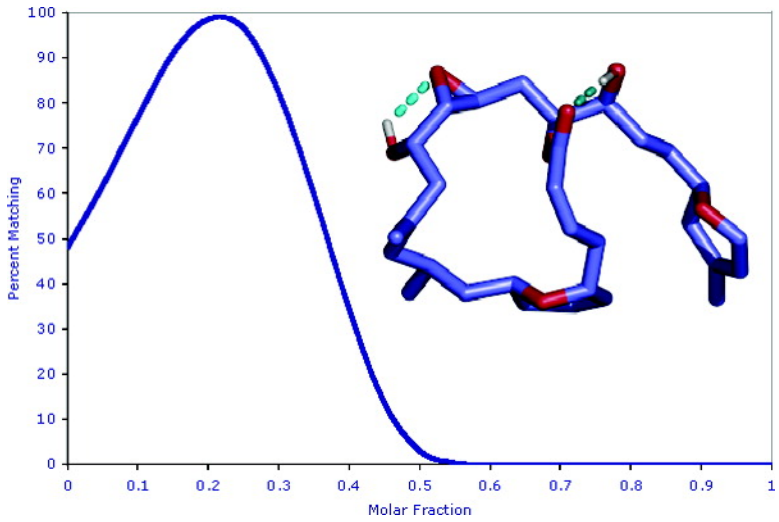


## More About This Article

Additional resources and features associated with this article are available within the HTML version:

- Supporting Information
- Links to the 6 articles that cite this article, as of the time of this article download
- Access to high resolution figures
- Links to articles and content related to this article
- Copyright permission to reproduce figures and/or text from this article

View the Full Text HTML

J|A|C|S
ARTICLES
Published on Web 08/25/2005

# Conformations of Laulimalide in DMSO-$d_6$

Pahk Thepchatri,[†] Daniel O. Cicero,[‡] Edith Monteagudo,[§] Arun K. Ghosh,[||] Ben Cornett,[†] Eric R. Weeks,[⊥] and James P. Snyder*[,†]

*Contribution from the Department of Chemistry, Emory University, Atlanta, Georgia 30322, NMR Laboratory, Faculty of Chemical Sciences and Technologies, University of Rome "Tor Vergata"; Istituto di Richerche di Biologia Molecolare P. Angeletti, 00040 Pomezia, Italy, Department of Chemistry, University of Illinois at Chicago, Chicago, Illinois 60607, and Department of Physics, Emory University, Atlanta, Georgia 30322*

Received November 24, 2004; E-mail: snyder@euch4e.chem.emory.edu

***Abstract:*** Laulimalide is one of the newest naturally occurring macrolides known to act as a microtubule stabilizing agent with properties similar to Taxol. It also stands as being one of the most flexible with 18 rotatable bonds. This large number of rotatable bonds allows for approximately $3^{18}$ potential conformers. To examine the conformational energy surface of laulimalide, we have performed an NAMFIS deconvolution analysis for laulimalide in DMSO-$d_6$. The latter has been supplemented with a post-NAMFIS energy analysis at the Becke3LYP/6-31G* level that examines the opposing effects of internal hydrogen bonding and *syn*-pentane interactions. In this way, we have identified 15 laulimalide conformations that can be classified into 5 different families: Supine, Convex, Cobra, Stretch, and Concave motifs.

## Introduction

Laulimalide (**1**) is an 18-membered macrolide isolated from two sponges indigenous to the Asian coastline.[1] The compound's total synthesis has been achieved by a number of routes.[2] The potential antitumor properties of the compound follow from the ability to stabilize microtubules and thereby disrupt tumor cell proliferation in a fashion that resembles the clinical anticancer agent Taxol.[3] A small number of other structurally diverse natural products under investigation as antitumor agents behave similarly and appear to exert their bioeffect by binding at the Taxol site on the $\beta$-tubulin ($\beta$-TB) protein: epothilone (**2**), discodermolide, eleutherobin, and the sarcodictyins.[4]

Although laulimalide is only one-fifth as potent as Taxol in drug-sensitive laboratory cell lines, it is 100 times more potent in multidrug-resistant cells. Moreover, the compound is able to block growth in cell lines resistant to Taxol and epothilone arising from the induction of specific mutations in $\beta$-tubulin (TB).[3,5] Thus, laulimalide is provisionally capable of escaping resistance arising from the two principle mechanisms, the operation of P-glycoprotein (Pgp)-mediated multi-drug resistance and induced tubulin mutations. Until very recently, the in vitro and cellular potencies of **1**, its resistance profile, and evidence that TB is a critical target have led to the general assumption that laulimalide binds a site on TB that is common to Taxol, the structurally similar epothilones (**2**), and the other drugs mentioned above. Surprisingly, Prior and co-workers have shown that laulimalide complexes tubulin in a 1:1 stoichiometry

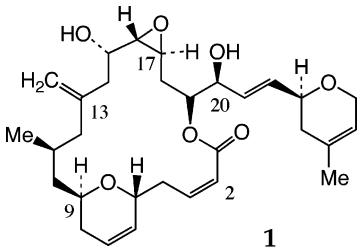


**1**

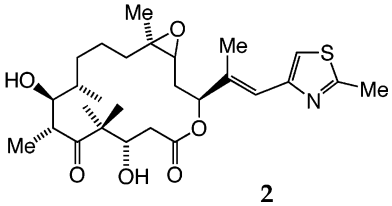


**2**

[†] Department of Chemistry, Emory University.
[‡] University of Rome "Tor Vergata".
[§] Istituto di Richerche di Biologia Molecolare P. Angeletti.
[||] University of Illinois at Chicago.
[⊥] Department of Physics, Emory University.

(1) Corley, D. G.; Herb, R.; Moore, R. E.; Scheuer, P. J.; Paul, V. J. *J. Org. Chem.* **1988**, *53*, 3644−3646.
(2) Ghosh, A. K.; Wang, Y. *J. Am. Chem. Soc.* **2000**, *122*, 11027−11028. Ghosh, A. K.; Wang, Y.; Kim, J. T. *J. Org. Chem.* **2001**, *66*, 8973−8982. Enev, V. S.; Kaehlig, H.; Mulzer, J. *J. Am. Chem. Soc.* **2001**, *123*, 10764−10765. Mulzer, J.; Öhler, E. *Angew. Chem., Int. Ed.* **2001**, *40*, 3842−3846. Paterson, I.; De Savi, C.; Tudge, M. *Org. Lett.* **2001**, *3*, 3149−3152. Wender, P. A.; Hegde, S. G.; Hubbard, R. D.; Zhang, L. *J. Am. Chem. Soc.* **2002**, *124*, 4956−4957. Crimmins, M. T.; Stanton, M. G.; Allwein, S. P. *J. Am. Chem. Soc.* **2002**, *124*, 5958−5959. Nelson, S. G.; Cheung, W. S.; Kassick, A. J.; Hilfiker, M. A. *J. Am. Chem. Soc.* **2002**, *124*, 13654−13655. Ahmed, A.; Hoegenauer, E. K.; Enev, V. S.; Hanbauer, M.; Kaehlig, H.; Ohler, E.; Mulzer, J. *J. Org. Chem.* **2003**, 68, 3026−3042. Gallagher, B. M., Jr.; Fang, F. G.; Johannes, C. W.; Pesant, M.; Tremblay, M. R.; Zhao, H.; Akasaka, K.; Li, X. Y.; Liu, J.; Littlefield, B. A. *Bioorg. Med. Chem. Lett.* **2004**, *14*, 575−579.
(3) Mooberry, S. L.; Tien, G.; Hernandez, A. H.; Plubrukarn, A.; Davidson, B. S. *Cancer Res.* **1999**, *59*, 653−660.
(4) Jiménez-Barbero, J.; Amat-Guerri, F.; Snyder, J. P. *Curr. Med. Chem.* **2002**, *2*, 91−122.
(5) Pryor, D. E.; O'Brate, A.; Bilcer, G.; Díaz, J. F.; Wang, Y.; Wang, Y.; Kabaki, H.; Jung, M. K.; Andreu, J. M.; Ghosh, A. K.; Giannakakou, P.; Hamel E. *Biochemistry* **2002**, *41*, 9109−9115.


**10.1021/ja042890e CCC: $30.25** 

with radiolabeled Taxol, suggesting that laulimalide and Taxol disable TB's normal function from different sites on the protein.[5] Most recently peluroside A, another potent cytotoxin isolated from a New Zealand sponge, has also been shown to stabilize microtubules but to bind to a site coincident with or overlapping that occupied by laulimalide.[6]

The present work seeks to develop an understanding of the conformational profile for **1** in solution. In part this is to address the observation that despite the superficial structural resemblance between **1** and **2** and their similar capacities for stabilizing microtubules, the structural similarity is not reflected in their respective interactions with the tubulin protein. Within the expansive taxoid pocket on $\beta$-tubulin, the works of Snyder,[7] Lowe,[8] Nettles,[9] and colleagues show that paclitaxel and epothilone A share few common contacts within the binding pocket. It would appear that the binding of small molecules to tubulin is far more complex and interesting than classic pharmacophore models would suggest. Seen from the perspective of hindsight, it is perhaps not surprising that subtle differences in structure and polarity dictate that laulimalide not only binds to an alternative site on tubulin but also causes a similar polymerization response by the protein. This is consistent with the observation that **1**, unlike Taxol and epothilone B, is unable to form the 2-D $Zn^{2+}$ stabilized sheets necessary for its structural determination by electron microscopy; instead 3-D microtubules are formed.[10]

Herein, we describe a deconvolution of the average structure of laulimalide in DMSO-$d_6$ with the 2-D NMR NAMFIS procedure (NMR Analysis of Molecular Flexibility in Solution)[11,12] to deliver 15 conformations with estimated populations ranging from 1.3 to 17.2%. These fall into five families with approximate populations between 7 and 27%. The procedure bypasses many of the pitfalls[12,13] associated with using force-field energies as a guide to conformational stability for molecules with the complexity of laulimalide. In addition, the final set of 15 conformations arose by performing several post-NAMFIS evaluations of the conformers in an attempt to ensure that they are both chemically reasonable and energetically viable.

## Materials and Methods

**Averaged NMR Spectrum of Laulimalide (1).** Laulimalide was assigned by a combination of 2D $^1$H and $^1$H−$^{13}$C experiments acquired on a Bruker Avance spectrometer operating at 600 MHz and equipped with a z-shielded gradient triple resonance probe. Spectra were processed using NMRPipe[14] and analyzed using the NMRView[15] software packages. The sample was prepared by dissolving 1.7 mg of laulimalide in 0.5 mL of DMSO-$d_6$ (Aldrich). $^1$H and $^1$H−$^{13}$C two-dimensional (2D) spectra (DQF-COSY, HOHAHA, ROESY, HMQC)[16] were accumulated at 298 K. $^1$H and $^{13}$C assignments (chemical shifts and $^3J_{HH}$) are provided in Tables S1 and S2 of the Supporting Information (SI).

***Table 1.*** ROESY-derived Distances of Laulimalide (**1**) in DMSO-$d_6$[a,b] (Å)

| | | r | | | r | | | r |
|---|---|---|---|---|---|---|---|---|
| H2 | H3 | 2.2 | H9 | H30 | 3.3 | H16 | H18b | 3.0 |
| H2 | H4a | 3.1 | H10a | H12a | 2.8 | H16 | H19 | 3.5 |
| H2 | H14a | 3.1 | H10a | H29a | 4.4 | H16 | H29a+H29b | 4.1 |
| H2 | H16 | 4.1 | H10a | H30 | 4.2 | H17 | H18a | 2.9 |
| H3 | H4a | 2.8 | H10b | H11 | 3.0 | H17 | H18b | 2.6 |
| H3 | H4b | 2.6 | H10b | H12a | 3.2 | H17 | H19 | 2.4 |
| H3 | H5 | 2.4 | H10b | H12b | 2.5 | H17 | H29b | 4.1 |
| H3 | H6+H7 | 3.2 | H10b | H30 | 3.5 | H18a | H18b | 1.8 |
| H4a | H4b | 1.8 | H11 | H12a | 2.5 | H18a | H20 | 3.1 |
| H4a | H6+H7 | 3.4 | H11 | H29a+H29b | 3.7 | H18a | H21 | 3.4 |
| H4b | H5 | 2.5 | H11+H12b | H29a | 2.7 | H18b | H19 | 2.5 |
| H4b | H6+H7 | 3.0 | H11 | H30 | 3.2 | H18b | H20 | 2.7 |
| H5 | H6+H7 | 2.8 | H12a | H12b | 1.8 | H19 | H20 | 2.2 |
| H5 | H10a | 3.1 | H12a | H15 | 3.0 | H19 | H21 | 3.2 |
| H5 | H11 | 3.5 | H12a | H30 | 3.9 | H19 | H22 | 3.1 |
| H5 | H12b | 3.1 | H12b | H29a+H29b | 3.0 | H20 | H21 | 2.3 |
| H6+H7 | H8a | 2.8 | H12b | H30 | 2.9 | H20 | H22 | 2.4 |
| H6+H7 | H8b | 3.2 | H14a | H15 | 2.8 | H21 | H24a+H24b | 3.3 |
| H8a | H9 | 2.2 | H14a | H16 | 2.4 | H22 | H23 | 2.5 |
| H8a | H10b | 2.9 | H14a | H17 | 2.9 | H22 | H24a+H24b | 3.5 |
| H8b | H9 | 3.2 | H14a | H30 | 4.7 | H23 | H28 | 4.7 |
| H8b | H10b | 2.6 | H14b | H15 | 2.8 | H26 | H27a+H27b | 2.9 |
| H9 | H10a | 3.1 | H14b | H16 | 3.0 | H26 | H28 | 3.5 |
| H9 | H10b | 2.6 | H14b | H17 | 3.2 | H29a | H30 | 4.1 |
| H9 | H11 | 2.5 | H15 | H29a | 3.9 | H29b | H30 | 4.7 |
| H9 | H12a | 2.5 | H15 | H29b | 2.5 | | | |
| H9 | H12b | 2.7 | H16 | H18a | 2.4 | | | |

[a] Internal calibration distance: H-2 and H-3, 2.2 Å. [b] NOE error estimates are approximately 5%; See SI, Table S5.

DMSO was selected as the NMR solvent because laulimalide is insoluble in the biological solvent water at concentrations that allow a 2D analysis. For example, to obtain a complete assignment of the molecule in solution, it was necessary to obtain $^{13}$C to $^1$H correlations at natural abundance. DMSO-$d_6$ but not $D_2O$ permits this. An important question concerns the relevance of conformations identified in DMSO in the biological context. Our experience with another notoriously water-insoluble compound, Taxol, supports the idea of a redistribution of conformer population as a function of solvent rather than formation of completely different forms. For example, comparison of NAMFIS conformers in $CDCl_3$ and DMSO/$D_2O$ illustrates a very similar set of conformers with quite different populations.[17] Accordingly, we assert that any bioapplications of the 15 conformations presented in this work (see below) can safely utilize the structures but should use the populations with circumspection.

Five ROESY spectra were recorded at 70, 100, 150, 180, and 200 ms mixing times to check the linearity of the cross-relaxation buildup rate. Interproton distances were calculated using the initial rate approximation and an internal calibration distance between H-2 and H-3 of 2.2 Å. The acquisition times t1 and t2 for the ROESY experiments were 213 and 32 ms, respectively. Relaxation delay was set to 2s, and 80 scans were accumulated per t1 increment. The 79 NOE-derived distances and eight useful $^3J_{HH}$ spin−spin couplings obtained from the treatment are presented in Tables 1 and 2, respectively. While 15 $^3J_{HH}$ values were perceived, only 8 were sufficiently resolved to be used as constraints in the NAMFIS analysis (cf. SI, Table S2).

**Conformational Searches.** Jefford's crystal structure of **1**[18,19] was used as a starting point for all conformational searches. The latter

(6) Gaitanos, T. N.; Buey, R. M.; Diaz, J. F.; Northcote, P. T.; Teesdale-Spittle, P.; Andreu, J. M.; Miller, J. H. *Cancer Res.* **2004**, *64*, 5063−5067.
(7) Snyder, J. P.; Nettles, J. H.; Cornett, B.; Downing, K. H.; Nogales, E. *Proc. Natl. Acad. Sci. U.S.A.* **2001**, *98*, 5312−5316.
(8) Lowe, J.; Li, H.; Downing, K. H.; Nogales, E. *J. Mol. Biol.* **2001**, *313*, 1045−1057.
(9) Nettles, J. H.; Li, H.; Cornett, B.; Krahn, J. M.; Snyder, J. P.; Downing, K. H. *Science* **2004**, *305*, 866−869.
(10) Cornett, B.; Nettles, J. H.; Downing, K. H.; Li, H.; Hamel, E.; Gapud, E. J.; Thepchatri, P.; Ghosh, A. K.; Snyder, J. P., submitted.
(11) Cicero, D. O.; Barbato, G.; Bazzo, R. *J. Am. Chem. Soc.* **1995**, *117*, 1027−1033.
(12) Nevins, N.; Cicero, D.; Snyder, J. P. *J. Org. Chem.* **1999**, *64*, 3979−3986.
(13) Ami Lakdawala, A.; Wang, M.; Nevins, N.; Liotta, D. C.; Rusinska-Roszak, D.; Lozynski, M. C.; Snyder, J. P. *BMC Chem. Biol.* **2001**, *1*, 2; http://www.biomedcentral.com/1472-6769/1/2.
(14) Delaglio, F.; Grzesiek, S.; Vuister, G. W.; Zhu, G.; Pfiezfer, J.; Bax, A. *J. Biomol. NMR* **1995**, *6*, 277−293.
(15) Johnson, B.; Blevins, R. A. *J. Biomol. NMR* **1994**, *4*, 603−614.
(16) Claridge, T. D. W. *High-Resolution NMR Techniques in Organic Chemistry*; Pergamon: NY, 1999.
(17) Ganesh, T.; Guza R. C.; Bane, S.; Ravindra, R.; Shanker, N.; Lakdawala, A. S.; Snyder, J. P.; Kingston, D. G. I. *Proc. Nat. Acad. Sci. U.S.A.* **2004**, *101*, 10006−10011; footnote p. 10009.
(18) Jefford, C. W.; Gernardinelli, G.; Tanaka, J.; Higa, T. *Tetrahedron Lett.* **1996**, *37*, 159−162.

***Table 2.*** Laulimalide (**1**) Proton−Proton Coupling Constants ($^3J_{HH}$) in DMSO-$d_6$ Utilized in the NAMFIS Analysis (Hz)

| | | | | $^3J_{HH}$ |
|---|---|---|---|---|
| H3 | C3 | C4 | H4b | 3.8 |
| H3 | C3 | C4 | H4a | 10.8 |
| H5 | C5 | C4 | H4a | 10.0 |
| H15 | C15 | C14 | H14a | 8.5 |
| H19 | C19 | C18 | H18b | 1.5 |
| H21 | C21 | C20 | H20 | 5.3 |
| H22 | C22 | C23 | H23 | 5.6 |

consisted of separate searches with the AMBER*, MM3*, and MMFF94s force fields in MacroModel 7.1[20] combined with the GBSA/$H_2O$ continuum solvent model.[21] Each force field was applied to three separate random-seeded searches of 75 000 MCMM (Monte Carlo Multiple Minimum)[21] steps to ensure that the potential energy surface was fully explored using the TNCG algorithm. The global minimum was found at least 12 times during the 75 000-step searches for each force field (SI, Table S3). Still et al. have suggested that locating the global minimum 7−12 times represents a thorough search of a molecule's potential energy surface.[20] The minimized conformers from the triplicate runs were then combined and fully optimized to convergence with their respective force fields using the FNMR algorithm and a 6.2 kcal/mol (26.0 kJ/mol) energy cutoff. Duplicate conformations were eliminated during this step.

Optimization of the crystal structure with each force field and subsequent superposition of the original crystal conformation demonstrated no significant conformational changes. However, the energy of the optimized experimental form proved to be 3−8 kcal/mol above the global minimum on the basis of force field energy differences (2.9, 3.5, and 7.6 kcal/mol for MMFF94s, AMBER*, and MM3*, respectively). The comparison illustrates that the conformational energy surface of laulimalide, like Taxol, is not represented uniformly by the present force fields.[22] A strong contributor to this outcome is undoubtedly that the three molecular mechanics procedures treat the electrostatic interactions between the five well-separated polar groups in **1** differently. [22]

Multiple force field optimizations followed by combination of all optimized structures led to a total of 15 093 fully optimized conformations. A search of this conformer pool using the FILTR function in MacroModel 6.5[20] was performed to ensure the presence of the empirically determined X-ray crystal conformation.[17] Thus, 10 backbone torsional angles taken from the crystal conformation with a ±25° window were used to extract compatible conformers from the pool. Of the 55 structures located, eight proved to correspond to the conformation presented by the X-ray structure, albeit with small torsional deviations in the backbone and variations in the two OH conformations. Superposition of the eight structures with the solid state form ensures that they correspond to the same conformation (cf. SI, Figure S1).

**Conformational Clustering.** As mentioned above, the multiple force field optimization procedure generated 15 093 structures for the conformational pool. Since the NAMFIS software cannot process this volume of structures due to its inability to dynamically allocate memory, XCluster v1.6[23] was employed to group conformations into a more manageable set of structurally related classes. The program calculates pairwise rms atomic displacements for a user-specified set of atoms following rigid-body superposition as the distance between a pair of structures.[24] Good clusters are characterized by short intercluster distances, one structure from each cluster selected to represent that cluster. In the present case, XCluster was instructed to group structures with similar hydrogen placement with the exclusion of hydroxyl hydrogens. This action reduced the number of structures in the conformational pool from 15 093 to 5496. Of the original eight conformers that correspond to the crystal structure, three survive. To complement these for the NAMFIS analysis (see below), the X-ray conformation with all heavy atom torsions fixed to solid-state values was optimized with the MMFF force field and added to the reduced pool to give a total of 5497 structures.

**NAMFIS.** A minimum of 18 rotatable bonds in laulimalide suggests the existence of families of widely varying conformations, ones that interconvert rapidly in solution by dynamic equilibrium. Like a number of related methods,[25] NAMFIS is an approach that deconvolutes the averaged NMR spectrum of a compound into weighted contributions from different conformers.[11] NAMFIS performs a least-squares fit of the ROE-determined proton−proton distances and $^3J_{HH}$'s against the same data extracted from the database of conformers. The procedure maximizes the match between experimental and computed variables by employing the E04UCF NAG FORTRAN Library Routine.[26] This is equivalent to minimizing the sum of square differences between the variables. Goodness of fit is expressed by a function defined as SSD (sum of square differences).[11,12] Unlike methods that vary a single structure until it fits the geometric constraints (e.g., constrained simulated annealing or restrained molecular dynamics), this approach varies the mole fraction of each fully optimized conformer until a "best fit" of the entire dataset is determined.

**NAMFIS - Karplus Equation.** Haasnoot, De Leeuw, and Altona have developed an extended Karplus equation describing the relationship between dihedral angles and $^3J_{HH}$ based on experimental NMR data.[27] The six-term expression (eq 1), including substituent electronegativity parameters, was presented with five different parameter sets (A−E). The most accurate parametrization involving the largest number of substitutents (E) has been implemented in the current NAMFIS methodology and applied to the laulimalide problem.

$$^3J_{HH} = P_1 \cos^2\phi + P_2 \cos\phi + P_3 + \Sigma\Delta\chi_1\{P_4 + P_5 \cos^2(\varsigma\cdot\phi + P_6\cdot|\Delta\chi_1|)\} \quad (1)$$

**NAMFIS - Results.** The 5497 laulimalide structures were processed to identify 22 conformations above a mole fraction of 0.01 that accommodate the NMR data with estimated populations ranging from 1.3 to 17.2%. (cf. Table 3). This set of structures delivers a satisfying sum of square differences (SSD = 52) between best-fit and computed variables.[11,12] Of the structures extracted by this methodology, one corresponds to the crystal structure[18] at a population of 1.5%, though it differs slightly in the orientation of the side-chain terminal dihydropyran ring (Figure 1). As a final check on the calculation, one additional analysis using a modified version of the NAMFIS program was applied to treat all 15 093 conformations plus the X-ray form by an incremental

(19) Bruno, I. J.; Cole, C.; Edgington, P. R.; Kessler, M.; Macrae, C. F.; McCabe, P.; Pearson, J.; Taylor, R. *Acta Crystallogr.* **2002**, *B58*, 289−397. Allen, F. H. *Acta Crystallogr.* **2002**, *B58*, 380−388; www.ccdc.cam.ac.uk/.
(20) Mohamadi, F. R.; Richards, N. G. J.; Guida, W. C.; Liskamp, R.; Lipton, M.; Caufield, C.; Chang, G.; Hendrickson, T.; Still, W. C. *J. Comput. Chem.* **1990**, *11*, 440−467; www.schrodinger.com/Products/macromodel.html.
(21) Still, W. C. T.; Tempczyk, A.; Hawley, R. C.; Hendrickson, T. *J. Am. Chem. Soc.* **1990**, *112*, 6127−6129.
(22) Lakdawala, A.; Wang, M.; Nevins, N.; Liotta, D. C.; Rusinska-Roszak, D.; Lozynski, M. C.; Snyder, J. P. *BMC Chem. Biol.* **2001**, *1*, 2; http://www.biomedcentral. com/1472−6769/1/2.
(23) Shenkin, P. S.; McDonald, D. Q. *J. Comput. Chem.* **1994**, *15*, 899−916.
(24) Kabsch, W. A. *Acta Crystallogr.* **1976**, *A32*, 922−923. Kabsch, W. A. *Acta Crystallogr.* **1978**, *A34*, 827−828
(25) Landis, C.; Allured, V. S. *J. Am. Chem. Soc.* **1991**, *113*, 9493−9499. Landis, C. R.; Luck, L. L.; Wright, J. M. *J. Magn. Reson., Ser. B* **1995**, *109*, 44−59. Wright, J. M.; Landis, C. R.; Ros, M. A. M. P.; Horton, A. D. *Organometallics* **1998**, *17*, 5031−5040. Nikiforovich, G. V.; Vesterman, B. G.; Betins, J. *Biophys. Chem.* **1988**, *31*, 101−106. Nikiforovich, G. V.; Kover, K. E.; Kolodziej, S. A.; Nock, B.; George, C.; Deschamps, J. R.; Flippen-Anderson, J. L.; Marshall, G. R. *J. Am. Chem. Soc.* **1996**, *118*, 959−969. Nikiforovich, G. V.; Kover, K. E.; Zhang, W.-J.; Marshall, G. R. *J. Am. Chem. Soc.* **2000**, *122*, 3262−3273. Mierke, D. F.; Kurz, M.; Kessler, H. *J. Am. Chem. Soc.* **1994**, *116*, 1042−1049. Cuniasse, P.; Raynal, I.; Yiotakis, A. *J. Am. Chem. Soc.* **1997**, *119*, 5239−5248.
(26) Numerical Algorithms Group (NAG) libraries: http://www.nag.co.uk/numeric/fl/ FLdescription.asp.
(27) Haasnoot, C. A. G.; De Leeuw, F. A. A. M.; Altona, C. *Tetrahedron* **1980**, *36*, 2783−2792.

***Table 3.*** NAMFIS Populations and Relative Free Energies, 298 K; Single-Point Becke3LYP/6-31G* Relative Energies[a]

| | | $\Delta E$(rel), kcal/mol | |
|---|---|---|---|
| conformer | pop, % | $\Delta G$(DMSO)[b] | $\Delta E$(calc)[a] |
| 1 | 17.2 | 0.0 | 0.0 |
| 2 | 12.2 | 0.2 | 1.4 |
| 3 | 9.7 | 0.3 | 1.3 |
| 4 | 7.5 | 0.5 | 2.0 |
| 5 | 5.7 | 0.7 | 2.5 |
| 6 | 5.1 | 0.7 | 2.6 |
| 7 | 4.9 | 0.7 | 1.6 |
| 8 | 4.8 | 0.8 | 8.9[c] |
| 9 | 4.2 | 0.8 | 4.7 |
| 10 | 3.8 | 0.9 | 10.7[c] |
| 11 | 3.3 | 1.0 | 11.3[c] |
| 12 | 2.6 | 1.1 | 12.8[c] |
| 13 | 2.5 | 1.1 | 4.7 |
| 14 | 2.1 | 1.2 | 5.0 |
| 15 | 1.9 | 1.3 | 4.5 |
| 16 | 1.6 | 1.4 | 6.4[c] |
| 17 | 1.6 | 1.4 | 8.4[c] |
| 18 | 1.6 | 1.4 | 3.1 |
| 19 | 1.5 | 1.4 | 1.0 |
| 20 | 1.4 | 1.5 | 3.9 |
| 21 | 1.4 | 1.5 | 2.0 |
| 22 | 1.3 | 1.5 | 10.2[c] |

[a] All conformers were reoptimized with the MMFF94s force field by applying a flat-bottom potential with a force constant of 2060 kJ/mol to all heavy atoms. [b] Derived from the estimated populations by a Boltzmann distribution at 300 K. [c] High energy conformations eliminated as part of the NAMFIS pool.

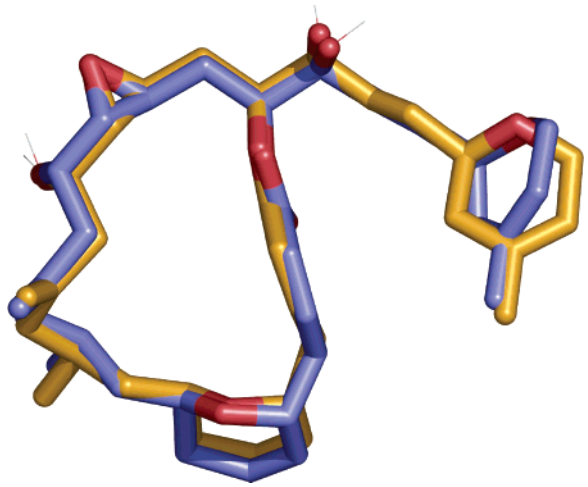

***Figure 1.*** X-ray structure (orange) superimposed by a low population NAMFIS conformer (blue). The two conformers differ by an RMSD of 0.5 Å for all heavy atoms.

conformer scanning procedure. The outcome was virtually identical to that derived from preclustering. Thus, for three separate runs using different increments (SI, Table S4) 20−23 conformers with populations from 1 to 18% were obtained (SSDs = 51), and the X-ray structure appeared at below 1%. For details of these runs and a discussion of errors in the NAMFIS procedure, see the SI.

**Energy Checks.** NAMFIS is a geometry engine that seeks to match distances and angles implied by the NMR data with those found in the conformational database. Any structure in the conformational pool that satisfies NMR-provided geometric conditions is a candidate ***without*** regard to structure quality or energy. If the energy cap specified in the conformational searches is too generous, defective or energy-rich structures can be selected by NAMFIS as a contributor to the solution of the fitting problem. By trial and error, we have settled on a 6.2 kcal/mol upper limit for our force-field conformational searches. This compromise appears to limit exposure of NAMFIS to sterically compromised structures, while allowing reasonable structures with overestimated relative energies[13] to be considered. Nonetheless, structures that are poorly represented by the applied force fields appear in the NAMFIS solution with an approximate frequency of 5−20%. For this reason, a final separate analysis must be performed to determine whether the NAMFIS conformations contain anomalous features that would identify them as unreasonably high in energy.

Three analyses were performed to address the energetic feasibility of the NAMFIS-selected laulimalide structures. The first involved a single-point density functional theory (DFT)[28] calculation for the 22 initial NAMFIS conformations with Becke3LYP/6-31G* as implemented in Gaussian.[29] Prior to this set of calculations, each of the 22 structures was reoptimized with the MMFF94s force field[30] by applying a flat-bottom potential with a force constant of 2060 kJ/mol to all heavy atoms.[31] Thus, each atom is allowed to move no more than 0.5 Å from its starting location ensuring that the torsional angles are maintained. In this way, all structures are placed on the same energy-geometry surface. The DFT energies vary from 1.0 to 12.8 kcal relative to the lowest energy structure of Table 3, conformer 1. The crystal structure falls within 1 kcal/mol of the latter. In combination with graphical inspection of the structures to ensure that no proton−proton distances fall below the sum of the van der Waals radii, we take energies from 0 to 5.0 kcal/mol as indication of the absence of chemically unreasonable features in the 22 conformers. Thus, we reject conformers 8, 10, 16, 17, and 22 as unreasonably high energy structures leaving a total of 15 viable forms.

Second, a single conformation with internal strain might be preferred in solution if it is reinforced sufficiently by intramolecular hydrogen bonding. In the case of laulimalide with two alcohol functionalities, a maximum of two hydrogen bonds can occur in any one conformation. In the NAMFIS set, two such conformations were identified, 1 (17.2%) and 7 (4.9%), Tables 3 and 4). In addition, nine conformers incorporate at least one internal H-bond (Table 4).

The third and final structure/energy evaluation involved a search for unfavorable *syn*-pentane or $A_{1,2}$-strain interactions in the NAMFIS-selected conformations of **1**. The latter correspond to structural fragments with potential for causing repulsive steric interactions between the terminal centers of a 5-carbon chain. Both Hoffmann[32] and Taylor[33,34] have argued that such contacts disqualify conformations that incorporate them from existing as viable solution structures. Six types we have considered are depicted in Figure S2 (cf. SI) and correlated with the 22 NAMFIS conformers in Table 4. Although over a third of the 22 structures (i.e., 10) currently carry at least 1 of these 6 *syn*-pentane types, only conformers 11, 12, and 22 were eliminated based on this criterion. Calculations in other cases imply that the energy penalty is negligible. Conformer 1 also contains one relatively high *syn*-pentane interaction but is ranked as the lowest relative energy in the NAMFIS-selected list. This is most certainly due to the fact that conformer 1 also sustains two intramolecular hydrogen bonds. As

(28) Becke, A. D. *Phys. Rev. A.* **1988**, *38*, 3098−3100.
(29) Frisch, M. J. T.; G. W.; Schlegel, H. B.; Scuseria, G. E.; Robb, M. A.; Cheeseman, J. R.; Zakrzewski, V. G.; Montgomery, J. A., Jr.; Stratmann, R. E.; Burant, J. C.; Dapprich, S.; Millam, J. M.; Daniels, A. D.; Kudin, K. N.; Strain, M. C.; Farkas, O.; Tomasi, J.; Barone, V.; Cossi, M.; Cammi, R.; Mennucci, B.; Pomelli, C.; Adamo, C.; Clifford, S.; Ochterski, J.; Petersson, G. A.; Ayala, P. Y.; Cui, Q.; Morokuma, K.; Malick, D. K.; Rabuck, A. D.; Raghavachari, K.; Foresman, J. B.; Cioslowski, J.; Ortiz, J. V.; Baboul, A. G.; Stefanov, B. B.; Liu, G.; Liashenko, A.; Piskorz, P.; Komaromi, I.; Gomperts, R.; Martin, R. L.; Fox, D. J.; Keith, T.; Al-Laham, M. A.; Peng, C. Y.; Nanayakkara, A.; Gonzalez, C.; Challacombe, M.; Gill, P. M.; Johnson, B.; Chen, W.; Wong, M. W.; Andres, J. L.; Gonzalex, C.; Head-Gordon, M.; Replogle, E. S.; Pople. J. A. *Gaussian 98*, revision A.7.; Gaussian Inc: Pittsburgh, PA, 1998.
(30) (a) Halgren, T. A.; Nachbar, R. B. *J. Comput. Chem.* **1996**, *17*, 587−615. (b) Halgren, T. A. *J. Comput. Chem.* **1999**, *20*, 730−748. (c) cf. www.schrodinger.com/macromodel2.html.
(31) Perola, E.; Charifson, P. S. *J. Med. Chem.* **2004**, *47*, 2499−2510.
(32) Hoffmann, R. W. *Angew. Chem., Int. Ed. Engl.* **1992**, *31*, 1124−1134.
(33) Taylor, R. E.; Zajicek, J. *J. Org. Chem.* **1999**, *64*, 7224−7228.
(34) Taylor, R. E.; Chen, Y.; Galvin, G. M.; Pabba, P. K. *Org. Biomol. Chem.* **2004**, *2*, 127−132.

***Table 4.*** *syn*-Pentane or $A_{1,2}$-Strain Interactions for the NAMFIS Conformers Quantified by Energy Differences between Folded and Extended Molecular Fragments (kcal/mol); Numbers of Intramolecular Hydrogen Bonds Per Conformer

| | B3LYP/6-31G* | | | |
|---|---|---|---|---|
| conformer | single-point[a] | DFT opt[b] | *syn*-p type | no. H-bonds |
| 1 | 2.7 | 2.3 | I | 2 |
| 2 | - - - | - - - | | 0 |
| 3 | 0 | 1.6 | III | 1 |
| 4 | - - - | - - - | | 1 |
| 5 | 0.1 | 0.1 | II | 0 |
| 6 | - - - | - - - | | 0 |
| 7 | - - - | - - - | | 2 |
| 8 | - - - | - - - | | 1 |
| 9 | - - - | - - - | | 0 |
| 10 | - - - | - - - | | 0 |
| 11 | 2.6 | 2.0 | IV | 0 |
| 12 | 2.9 | 2.3 | I, VI | 0 |
| 13 | - - - | - - - | | 1 |
| 14 | - - - | - - - | | 1 |
| 15 | - - - | - - - | | 1 |
| 16 | - - - | - - - | | 1 |
| 17 | - - - | - - - | | 0 |
| 18 | −1.7 | −2.0 | IV | 0 |
| 19 | - - - | - - - | | 1 |
| 20 | 0.2 | 1.4 | V | 0 |
| 21 | - - - | - - - | | 0 |
| 22 | 0.1 | 0.3 | II, III | 1 |

[a] MMFF94s geometries; DFT energies: B3LYP/6-31G*//MMFF94s. [b] B3LYP/6-31G*//B3LYP/6-31G*

implied by Table 4, energies of the latter readily compensate for *syn*-pentane contacts.

A final point concerns the validity of the NAMFIS analysis once seven high energy conformers have been removed. We have tested this in two ways. First, we have resubmitted the 22 and 15 conformation datasets to separate NAMFIS analyses to back-calculate the data. With one exception at 1.0 Å, all 79 NOE distances are predicted to differ from the experimental values by <1.0 Å, and all $^3J_{HH}$'s are predicted within 1 Hz for both cases. The SSDs of 52 and 54, respectively, are virtually identical to that from the original calculation with 5497 conformers; SSD = 51. A similar analysis for the subset of the five leading conformations from each of the conformer classes preserves the characteristics of the 15 and 17 conformer runs, although the fit of the data is degraded (SSD = 153; cf. SI, Table S6). A second series of NAMFIS forecasts examined the sensitivity of the family populations to variations of the experimental dataset. Once again, the 15 final conformers preserve family characteristics and populations within a few % of the full 22 conformer set (cf. SI, Table S7).

**Graphics.** The majority of the illustrations in this paper have been rendered with Delano's program PyMol,[35] while Figure 8 was prepared with Maestro.[36]

## Families of Laulimalide Conformations in DMSO-$d_6$

The final 15 NAMFIS conformers can be grouped into 5 structural motifs (Table 5) generalized by the symbolic structure depicted in Figure 2. Names of the classes were inspired by the convex or concave nature of the lactone ring and the orientation of the side chain relative to the terminal ring. As will be depicted below, superposition of members of a given class does not result in perfectly aligned structures. Rather, the overlap shows the viewer the preferred arrangements of functionality in molecular space.

(35) DeLano, W. L. *The PyMOL Molecular Graphics System*; DeLano Scientific: San Carlos, CA, USA, 2002. http://pymol.sourceforge.net/.
(36) Maestro 7.0 Schrodinger, LLC, New York, 1999−2005. http://www.schrodinger.com/.

***Table 5.*** Total Populations for the NAMFIS Motif Types from the Final 15 Conformers Excluding Structures with 0.01 Mole Fraction

| pop, %[a] | motif | members |
|---|---|---|
| 33.7 | supine | 3, 4, 6, 19, 20, 21 |
| 30.0 | convex | 1, 7, 18 |
| 20.8 | stretch | 2, 9 |
| 8.2 | concave | 13, 14, 15 |
| 7.2 | cobra | 5 |

[a] Populations are the normalized sum of the 15 individual conformer populations following the post-NAMFIS energy filtering of seven high-energy structures.

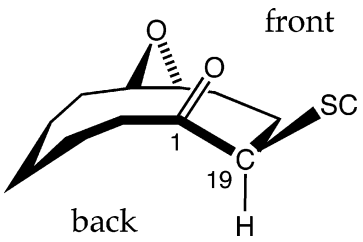


***Figure 2.*** The overall spatial features of the majority of laulimalide conformers are characterized by a convex ring shape and by various orientations of the side chain relative to the macrocyclic ring.

The first two motifs listed in Table 5 share many conformational features with the solid-state structure of **1**. Those most similar to the crystal structure, the "Supine" family, are populated at 34%. The second most populated class ("Convex" 30%) is similar to the Supine group in terms of side chain placement and most parts of the main ring except for the orientation of the carbonyl attached to C-1 as shown in Figure 3. The experimentally determined structure (green) directs the carbonyl oxygen behind the plane of the paper, while conformer 1 directs it above the same plane. Conformations with carbonyl placement in the Supine motif tend to show a flatter macrolide ring by comparison with the Convex family of conformations.

**Supine Motif.** Although this is the most plentiful motif among the NAMFIS conformers, its top contributor is only the third most populated structure (conformer 3, Table 3). An NAMFIS-selected variant on the crystal conformer is included in the family. The latter exhibits a somewhat flat lactone ring with the side chain curled in the same approximate plane as the ring (Figure 3). Characterization of the macrolide ring as "flat" is relative to the curled conformations displayed by the Convex and Concave motifs discussed below. The only intramolecular hydrogen bonding interaction possible in this class is between the epoxide oxygen and the main ring hydroxyl group. Three conformers in the set sustain this bond (#3, #4, #19, Table 4). The side chain hydroxyl group points to the front face, while the lactone carbonyl points to the back. The most flexible torsional segments appear between the terminal alkene of the main ring and the side chain ring (i.e., C-12−C-20). Figure 4 illustrates that most oxygen functionalities reside in similar regions of space, although the OH at C-15 is highly variable. Steric features are consistent from conformer to conformer.

**Convex Motif.** The Convex family is characterized by its macrocyclic lactone ring being more curled than observed in the Supine motif. As seen in Figures 2−5, the side chains of both forms sit alongside the edge of the main ring, but the rings themselves adopt spatially distinct shapes. The side-chain hydroxyl groups at C-20 are projected essentially orthogonal to the average plane of the macrocyclic ring. Two conformations

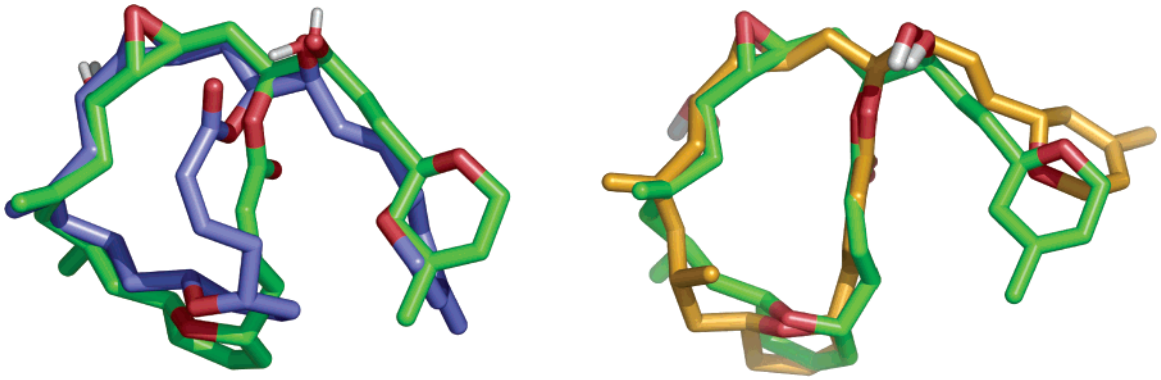

***Figure 3.*** Crystal structure (green) overlapped with most populated member of Convex family (blue) on left; crystal structure overlapped with most populated member of Supine family (orange) on right.

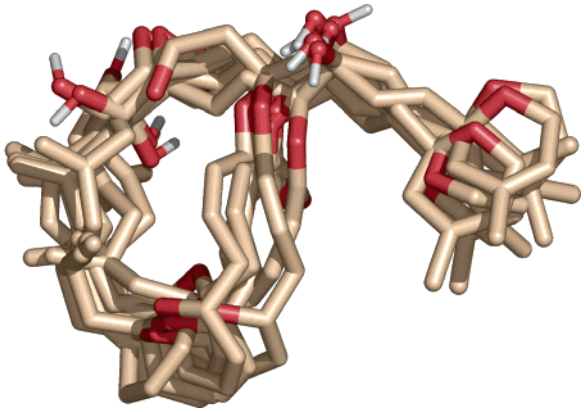

***Figure 4.*** Superposition of the members of the supine motif characterized by a lactone ring that is relatively in line with the plane of the paper. The C═O directed beneath the plane of the paper. The spatially variable C-15 OH is shown at the upper left.

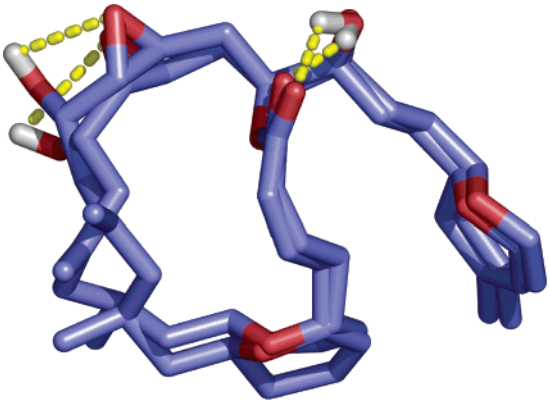

***Figure 5.*** Superposition of Convex conformations 1 and 7 (dark blue) characterized by a convex lactone ring, the C═O directed above the plane of the paper, and two internal hydrogen bonds (dashed).

in the Supine category (conformers 1 and 7) have the advantage of two intramolecular hydrogen bonds (Tables 4 and 5). Thus, not only does the C-15 OH reach the epoxide oxygen, but the C-20 OH and the C-1 carbonyl on the convex face of molecule likewise engage in H-bonding. NAMFIS and the DFT calculations are in accord in showing this motif to harbor the most highly populated and most energetically stable conformer, respectively.

**Stretch Motif.** This pool of two conformers makes up the third largest population from the NAMFIS analysis, although it contains the second most populated conformer (Table 3).

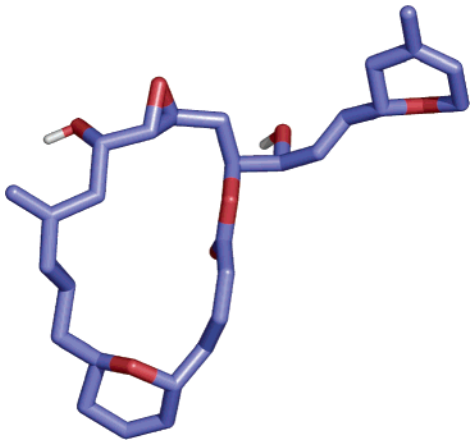

***Figure 6.*** The Stretch motif, ranking third in terms of family population, is illustrated by the second most populated NAMFIS conformation (#2).

Members of the class show a macrolide ring conformation similar to the Supine motif. However, this group of conformers deserves distinction because the side chains tend to stretch away from the lactone ring rather than neighbor it (Figure 6).

**Concave Motif.** The unique feature of this two-conformer motif is that the macrocyclic lactone ring adopts a concave shape by comparison with all other NAMFIS conformers (cf. Figure 4). In terms of oxygen placement, this family is most similar to the X-ray containing Supine family, in which the C-1 carbonyl is too distant from any hydroxyl to participate in hydrogen bonding. On the other hand, similar to the Convex family, the C-15 hydroxyl group is H-bonded to the epoxide oxygen (Figure 7).

C**obra Motif.** The fifth and final most populated rotational isomer pattern is dubbed the "Cobra" conformation. Unlike the Supine and Convex motifs, this family extends the side-chain terminal dihydropyran ring directly over the center of the face of the macrolide ring (Figure 8). The orientation is unique in that none of the other structures identified by NAMFIS orient the side chain in this manner.

Oxygen functionality in the lactone ring is distributed within a rather tight radius for the superposed Cobra structures. The width of the lactone ring for this conformer class is the greatest among the various motifs. One measure of the diameter of the macrolide ring is the distance between H-2 and H-16. While this value ranges from 7.5 to 8.3 Å for the Cobra subset, it varies between 3.9 and 6.1 Å for other motifs (Table 6). Finally, with the exception of conformer 22 with one hydrogen bond,

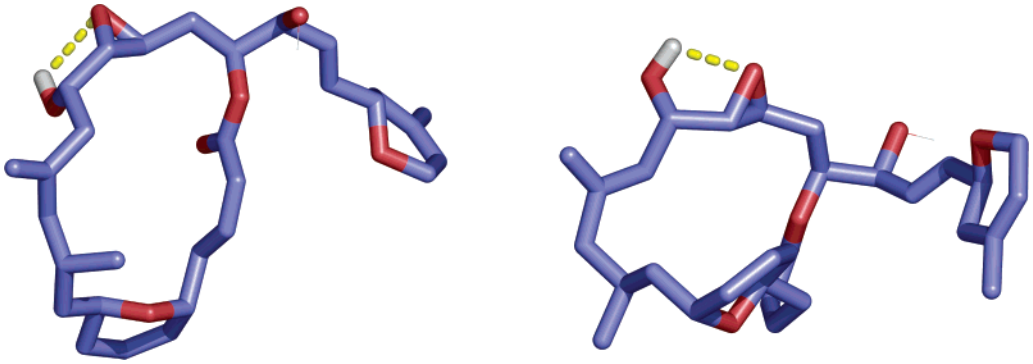

***Figure 7.*** Comparison of Supine (left) and Convex motifs (right). The C-15 OH is H-bonded to the epoxide oxygen in both classes; H-bonds dashed.

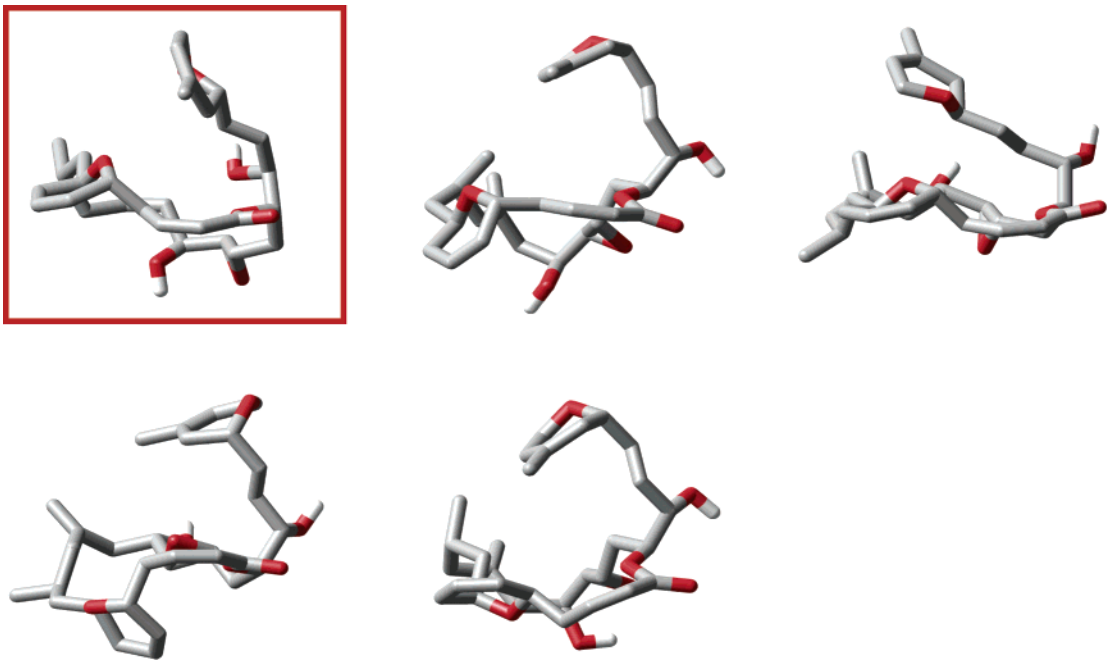

***Figure 8.*** The Cobra conformations; the side-chain dihydropyran ring is centered above the convex face of the lactone ring; side views. Of all the structures in this family, only the top-left structure (highlighted in red) was found to be energetically reasonable.

***Table 6.*** Comparison of H-2 to H-16 Interproton Distances for the Most Populated Conformers of Each Motif (cf. Table 7)

| conformer | *r*, Å |
|---|---|
| ROE(exp) | 4.1 |
| 1 | 3.9 |
| 2 | 3.9 |
| 3 | 5.1 |
| 12 | 6.1 |
| 5 | 7.6 |

there are no strong intramolecular associations observed for this conformer class.

**Matching Curves; Probability Analysis.** NAMFIS matching curves in general, and more specifically those in Figure 9, measure the ability of a set of computer-generated conformations to fit the geometric data provided by the NMR spectrum (interatomic distances and $^3J$-determined dihedral angles).[11] It should be noted that the *Y*-axis of the curves in Figure 9 records the degree of matching (see below) between a given conformer or conformer family and the data, while the *X*-axis reports the corresponding mole fraction. Three types of information are found on each curve. The first is the maximum point, arbitrarily assigned as 100% matching and defined as the "best fit" to the data. These values are recorded for each conformation and conformer family reported in Tables 3 and 5, respectively. The latter plus all other points under the curve correspond to the "feasible space" (see below) for a given conformer or family. Thus, the second readout of the curve is the total feasible space represented by the breadth of a curve at its base. For example, for the most populated Supine family (Figure 9B), feasible values for the existence of the family as perceived by the NMR experiment fall within the mole fraction range of 0.0−0.62. The curve states that a mole fraction of 0.62 accommodates almost none of the match associated with the best fit, while a mole fraction of 0.0 matches 78% of it. These values in the feasible solution can be regarded as the worst-case propagated error for the Supine family.

The third interpretive aspect of the matching curve is subjective. We take the half-width of each curve as a reasonable assessment of the probability that a structure or family of structures is found in the conformational equilibrium and regard highly probable solutions as those that fit the data with a matching of more than 80% of that derived for the best fit. Thus for the most populated Supine family, these range from a mole fraction of 0.02 to 0.38 bracketing the best fit at 0.27. When energetically unreasonable conformations are removed from the

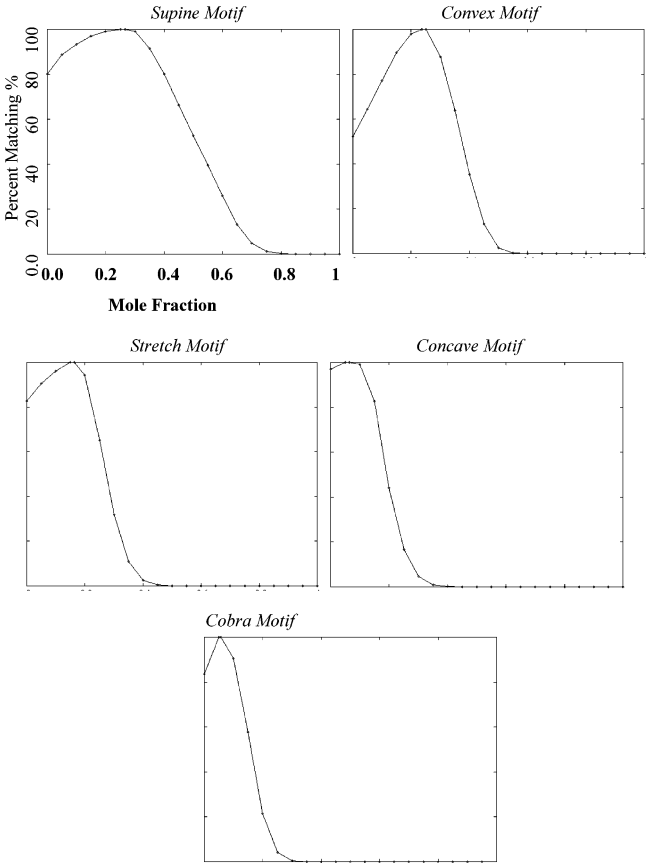


***Figure 9.*** Matching curves for each motif: Supine, Convex, Stretch, Concave, and Cobra; cf. Table 5. The *x*-axis reports a family's mole-fraction, and the *y*-axis, the degree of matching to the data (i.e., the SSD). The "best fit" solution satisfies all families simultaneously and corresponds to the maximum point on each curve.

original set (cf. Energy Checks above), the total mole fraction for this family rises to 0.34 (34% population; Table 5).[37]

To give the reader an appreciation for this analysis in some of its essential details, we briefly review the NAMFIS methodology. At the outset of the procedure, each structural parameter $A_i$ (NOE distance or $^3J$) is assigned a maximum error based on both experimental inaccuracies and approximations in the structure generation tools (Karplus equation and molecular mechanics methods). Thus, $\Delta A_i = \Delta A_i^{\text{exp}} + \Delta A_i^{\text{calc}}$.[11] Then, normalizing the mole fractions of all conformations ($n_c$) to 1 (i.e. 100%), a *feasible solution* is defined as the set of mole fractions that satisfies eq 1 for all the NMR parameters $n_p$.

$$A_i^{\text{exp}} - \Delta A_i + \leq \Delta A_i^{\text{calc}} \leq \Delta A_i^{\text{exp}} + A_i \qquad i = 1, n_p \quad (1)$$

The ensemble of all feasible sets of mole fractions constitutes the *feasible space* of the variables. By maximizing an appropriate function $F = f(x_k)$ within the constraints set by eq 1, it is possible to calculate the upper and lower limits of the feasible space for each mole fraction. The set of conformer-specific feasible spaces is an analytical solution for the complete feasible space, since it encloses all the possible distributions of conformers that are compatible with the available experimental evidence. When the latter is expressed in quantitative terms (i.e., specific interatomic distances and $^3J$'s), the feasible space can be quantified by matching the calculated and experimental quantities. The NAMFIS procedure defines the degree of matching ($M$) according to eq 2.

$$M = \prod_i \exp-\{{}^1/_2[(A_i^{\text{exp}} - A_i^{\text{calc}})/\Delta A_i]^2\} \qquad i = 1, n_p \quad (2)$$

Maximizing $M$ is equivalent to minimizing the sum of the square differences between $A_i^{\text{exp}}$ and $A_i^{\text{calc}}$. In practice, the magnitude of a mole fraction at a given value is evaluated by holding its population constant while allowing the population of all other conformations to vary within their feasible domains. The matching curve is constructed by performing this exercise in 0.2 mole fraction increments from 0 to 1. The mathematical and algorithmic details have been discussed previously.[11] It is important to recognize that this procedure rejects all matches that do not satisfy the condition of eq 1, that is, matches outside the error boundaries. Of all the feasible solutions, the mole fraction that exhibits the optimal fit of the data (highest value of M) is assigned a 100% value, the "best fit". This model only represents a single point in the $n_c$-dimensional feasible space defined by the mole fractions of all conformations satisfying eq 1. As mentioned above, however, the complete matching curve provides both a measure of the total feasible space that reproduces the data and a subjective probability regarding the existence of a given conformation or family thereof.

From the above discussion, it is clear that there is no unique solution to the problem of deconvoluting an averaged NMR spectrum into constituent conformations with specific and well-defined populations; the problem is indeterminate. On the other hand, it is also clear that one model of the conformational distribution within the feasible space matches the data best, while all others do so with decreasing quality. Without independent supporting data, it is unreasonable to suppose that a less than optimal data match more adequately represents the laulimalide conformational distribution than the best fit. Accordingly, we highlight these populations in Tables 3 and 5, although we do not claim to define an exact value for a given conformation or associated family. In principle, the treatment cannot unambiguously rule out a small or zero population for a given structure or class. The probablility of the latter is low, however, as it would generally occur for a rather poor fit of the NMR variables.

Returning to the families represented by the matching curves in Figure 9, we comment on their error profile. The half-widths of the curves from 80−100% fit of the data (i.e., 90%) are defined as highly probable solutions to the conformational problem. For the Supine, Convex, Stretch, Concave, and Cobra families, this corresponds to mole fraction windows of 0.36, 0.14, 0.16, 0.16, and 0.8, respectively. Using the best fit populations of Table 5, we estimate the population errors as follows: 34% ± 18, 30 ± 7, 21 ± 8, 8 ± 8, and 7 ± 4%, respectively. These rather generous error bars suggest that the Supine, Convex, and Stretch families are important contributors to the laulimalide conformational equilibrium. They likewise project that the low population Concave and Cobra families may or may not exist in DMSO-$d_6$, although the standard deviation treatment in the next paragraph definitely includes these forms.[38]

(37) The mole fraction of 0.27 (27% population) differs from the value of 0.34 (34%) recorded in Table 5 because the former refers to the original 22 NAMFIS conformers, while the latter refers to the final 15 conformers following the post-NAMFIS energy analysis.

(38) See the Supporting Information for further discussion on errors, error propagation, and interpretation of the NAMFIS matching curves.

The half-width analysis for the single conformations of Table 3 (see SI) suggests the first three play a role in solution, the identity of the rest being uncertain. The latter, however, makes up 61% of the mole fraction. While a complete specification of these particular conformers may be in doubt, the data-fitting outcome predicts that any replacement conformers will exhibit similar geometries.

In an independent attempt to assess error propagation and the viability of the NAMFIS conformations, we randomly varied each of the 87 geometric quantities derived from laulimalide's NMR analysis within its error boundaries and performed 19 subsequent NAMFIS analyses for a total of 20 data sets. While none of the individual conformations in Table 3 survived all 19 variations, the five families described above were returned in each replicate. The populations and standard deviations for the Supine, Convex, Stretch, Cobra, and Concave families were 31.4 ± 9.6, 23.7 ± 10.4, 16.4 ± 8.6, 16.7 ± 6.6, and 9.7 ± 4.9%, respectively. Thus the predicted values for each family motif exist well within their respective uncertainty values. These results parallel those derived from matching curve considerations, strengthen the proposition that the Supine and Convex forms are the dominant conformations in solution, and support the remaining three families as low population contributors. At the same time, this data analysis implies that no single conformation can be assigned with certainty. However, congruent with interpretation of the matching curve analysis, family integrity ensures that laulimalide conformations with very similar characteristics (e.g., similar functional group placement) are to be found in solution as representatives of the individual families.

## Summary and Conclusions

The combined NMR experiments and NAMFIS analysis demonstrate that laulimalide exists in a dynamic conformational equilibrium in solution consisting of at least four, maybe five, different families of rotational isomers. In order of predicted decreasing concentration, these have been named the Supine, Convex, Stretch, Cobra, and Concave motifs (Table 5). Seven of the 22 first-pass NAMFIS conformers can be rejected based on energy (Tables 3 and 5). Significantly, the X-ray conformation of laulimalide[18] is weakly present in the remaining 15 conformations that best fit the NMR data in DMSO-$d_6$, and the highest populated Supine family shares significant resemblance to it. While none of the Supine conformers are an exact match, they capture much of the spatial functionality of the crystal form.

All five conformational motifs deduced from the NAMFIS treatment present significantly different local minimum arrangements not easily deduced from the NMR time-averaged data alone. Perhaps the most unusual of these is the Cobra motif, which places the dihydropyran ring at the terminus of the laulimalide side chain above the center of a rather expanded macrocyclic lactone ring. From a broad perspective, the situation is reminiscent of Taxol,[39] discodermolide,[40] eleutherobin,[41] and epothilone.[6,7] Each of these natural products, like laulimalide, stabilize microtubules, promote tumor cell death and exist as a collection of rapidly equilibrating conformations sorted into a few families. In the cases of Taxol and epothilone, unique and efficacious anticancer agents, the NMR conformations have contributed to the formulation of an atomic model of the drug bound to its $\beta$-tubulin target[7,9] as a result of docking the structures into the low-resolution electron crystallographic density to identify that most compatible with it. Given the importance of identifying novel and resistance-free anticancer agents, and the potential role of structure-based molecular design to this end, we anticipate that the laulimalide conformers deduced during the course of this work will likewise play an influential role in determining the structure of the $\beta$-tubulin−laulimalide complex.

**Acknowledgment.** A.K.G. thanks the National Institutes of Health for partial support of this work. P.T., B.C., and J.P.S. are thankful to Professor Dennis C. Liotta (Emory University) for support of the work.

**Supporting Information Available:** Chemical shift assignments for **1**; NAMFIS tests and alternative runs; error estimates; strain calculations; Cartesian coordinates for the NAMFIS conformations. This material is available free of charge via the Internet at http://pubs.acs.org.

JA042890E

(39) Snyder, J. P.; Nevins, N.; Cicero, D. O.; Jansen, J. *J. Am. Chem. Soc.* **2000**, *122*, 724−725.
(40) Monteagudo, E.; Cicero, D. O.; Cornett, B.; Myles, D. C.; Snyder, J. P. *J. Am. Chem. Soc*. **2001**, *123*, 6929−6930.
(41) Cornett, B.; Monteagudo, E.; Cicero, D. O.; Cinel, B.; Anderson, R. J.; Roberge, M.; Milanesio, M.; Liotta, D. C.; Snyder, J. P., submitted.